ELSEVIER

Contents lists available at ScienceDirect

Combustion and Flame

journal homepage: www.sciencedirect.com/journal/combustion-and-flame





Double flame dynamics in hotspot ignition

Keisuke Akita ^{a,b,c}, Peng Zhao ^{a,*}, Youhi Morii ^b, Kaoru Maruta ^b

- ^a Department of Mechanical, Aerospace and Biomedical Engineering, UT Space Institute, University of Tennessee, Knoxville, TN 37388, USA
- b Institute of Fluid Science, Tohoku University, Sendai, Miyagi 980-8577, Japan
- ^c Graduate School of Engineering, Tohoku University, Sendai, Miyagi 980-8577, Japan

ARTICLE INFO

Keywords:
Hotspot
Cool flame
Double flame
Ignition
Low temperature chemistry
Spherical flame

ABSTRACT

Hotspot ignition is a key problem in fundamental flame initiation, combustion control and prevention of abnormal combustion phenomena. Depending on the characteristics of the hotspot and the thermochemical condition of the reactive mixture, subsequent reaction front initiated from a hotspot can vary substantially. The current paper focus on the dynamics and chemistry for one of the most complicated scenarios - hotspot induced double flames, which include a cool and a hot flame segment. This work adopts a recently developed compressible reacting flow simulation code COGNAC to investigate the initiation and propagation of double flame dynamics from hotspot ignition in a one-dimensional spherical coordinate. The results have shown that under atmospheric pressure, double flame initiation is not feasible for sufficiently small hotspot. Under elevated pressures, double flame can be initiated within a much wider hotspot window, exhibiting complex flame dynamics, such as variations in cool and hot flame bifurcation behaviors and their initiation locations. Analysis on thermochemical structure and dynamics of double flame has shown that the interaction of cool and hot flames in a double flame structure is inherently intermutual, in that the leading cool flame enhances trailing hot flame via thermal expansion effects.

1. Introduction

Hotspot induced flame initiation has been a crucial problem in both fundamental and applied combustion [1]. Active flame triggering for combustion phasing control in practical systems such as spark-ignition [2] and laser-ignition [3] is frequently modeled as hotspot ignition. Furthermore, undesired abnormal combustion phenomena in engines and turbines are frequently caused by hotspot ignition, such as engine knock [2], super knock [4], and low-speed pre-ignition [5]. Therefore, understanding of hotspot characteristics and the subsequent flame initiation processes plays a critical role for both active combustion control and prevention of abnormal combustion in practical power and propulsion systems.

Fundamentally, depending on the nature of the hotspot (e.g., size, peak temperature, gradient) and the thermal chemical condition of the local mixture, the consequence of hotspot ignition can be a regular hot flame, autoignition-assisted hot flame [6], spontaneous autoignition front propagation [7], cool flame [8], double flame [9], and detonation [10]. Among these reaction fronts, the direct initiation of double flame, including a hot and a cool flame segment, either coupled or decoupled, is

most complicated and least understood. Numerical simulation performed by Ju et al. [11] is a pioneering study to identify double flame formation from flame splitting for lean n-heptane/air in a specific 1D cylindrical configuration. With a relatively large size of hotspot, Zhao et al. [12] have found that a cool flame can always be involved in hotspot ignition in 1D planar configuration, for hot pockets with temperatures below, within, and beyond the negative-temperature coefficient (NTC) regime. Zhang et al. [8] examined effects of hotspot size and temperature on flame initiation in various DME/air mixtures, providing insights into the evolution of 1D planar premixed cool, double, and hot flames.

Experimentally, recent advances in flame measurement using shock tubes [13] and rapid compression machines [14] have made it feasible to observe the hotspot induced initiation and propagation of laminar flames in mixtures under elevated thermodynamic conditions. A key observation from the shock tube flame experiment includes multistage flame structures and non-monotonic temperature dependence of the flame speed in the NTC region for a n-heptane/O2/Ar/He mixture. Assisted by 1D [9] and 2D [15] numerical simulations, Zhang et al. provided explanations to the multilayer flame structure and

E-mail address: pzhao12@utk.edu (P. Zhao).

https://doi.org/10.1016/j.combustflame.2024.113660

 $^{^{\}ast}$ Corresponding author.

non-monotonic flame propagation by relating to the double flame concept.

Indeed, all these experimental and numerical studies have laid a solid background for double flame investigation. However, the dependence on geometry, thermodynamic condition, and hotspot characteristics for direct double flame initiation subject to curvature effects lacks systematic study and remains unclear. Such gap in double flame research is also partially attributed to the fact that the major physical components included in this problem, such as dynamics of spherical cool flame [16] and stretched hot flame subject to reaction progress effects [17,18], are not fully understood until very recently.

The objective of this study is therefore three-fold: first, we aim to identify the dependence of double flame initiation on hotspot sizes in 1D spherical coordinate. Second, we evaluate the effects from elevated pressure on spherical double flame initiation, especially novel combustion mode including complex flame bifurcation. Last, we demonstrate the inherent coupling in double flame dynamics, where we have found that the propagation of leading cool flame can be strongly affected by the burnt condition in the trailing hot flame. To the best of the authors' knowledge, this is the first work demonstrate novel combustion mode and inherent coupling in double flame dynamics by a spherical hotspot.

2. Numerical methods

We employed an in-house reacting flow simulation software, COGNAC (COmpressible Gas with Navier-Stokes And Combustion) [18] to investigate the initiation and propagation of spherical double flames. COGNAC solves the fully compressible governing equations with species, momentum, and energy conservation, accommodating detailed transport and chemistry [19]. To avoid redundancy and stay focused, we have not included them in the current manuscript. Finite volume method (FVM) is applied for spatial discretization. The monotonic upstream-centered scheme for conservation laws (MUSCL) [20] is utilized to ensure a third-order spatial accuracy. The numerical fluxes of convective terms are calculated by the Harten-Lax-van leer contact (HLLC) Riemann solver [21]. Second-order terms including the viscous force, heat conduction, and mass diffusion terms are calculated by second-order central difference scheme. Time integration is realized by the total variation diminishing (TVD) Runge-Kutta scheme with third-order accuracy [22]. Chemistry integration is achieved by a fast robust Jacobian-free minimum-error adaptation chemical-kinetic solver (MACKS) [23]. The simulation is sufficiently validated against Chemkin and other codes such as A-SURF [24], including spherical flame initiation and propagation. Further details regarding the numerical models and validation results are available in previous publications [18,25].

N-heptane, as a primary reference fuel, is adopted in the current paper, exhibiting both high and low temperature chemistry. A skeletal model with 88 species and 387 reactions [26] is adopted, which has been validated against flame speed and ignition delay in a wide range of thermodynamic conditions. The computational domain is in 1D spherical coordinate and has a radius of r = 6.0 cm. Within this domain, constant grid sizes of $\Delta r = 20 \, \mu m$ and $6 \, \mu m$ are applied for simulations at 1.0 and 10.0 atm, respectively, which has shown satisfactory grid independence. The grid size in our simulations is carefully chosen to ensure adequate resolution and grid independence of the flame front. Specifically, at least 10 grids are included within flame thickness, ensuring that the flame structure is accurately captured during evolution. Beyond the r = 6.0 cm domain, the grid size is gradually increased towards the right boundary to minimize the reflection of pressure waves. Symmetric and outlet boundaries are applied for the left ($r=0\ \mathrm{m}$) and right (approximately r = 10 m) boundaries, respectively.

We intentionally select 10 atm in the current study to provide practical insight for understanding pressure effects on double flame initiation. One major consideration is that ignition and flame initiation frequently occur at the end of compression stage either from piston or compressor, where the pressure is frequently around 10–15 bar. The much higher pressure in the later stage of these practical power systems is nevertheless induced by severe heat release from the intense combustion. Meanwhile, double flame initiation is significantly influenced by the difference in the ignition delay times of cool and hot flames, as governed by factors such as pressure, hotspot features, and mixture compositions. At pressures beyond 10 atm, due to increased collision frequency and chemical reactivity, the ignition delay times between them become shorter, causing a narrower window for double flame observation.

The flame initiation is achieved by the following hotspot temperature profile [24]:

$$T_H(r) = \Delta T \exp \left[-\left(\frac{r}{R_H}\right)^{\rm M} \right] + T_0$$
 (1)

where T_0 is ambient temperature, ΔT is temperature difference between hotspot central temperature, T_H , and ambient temperature, $T_0=700.0$ K, R_H is a hotspot radius, and M is a geometric parameter for the hotspot gradient. For simulations under atmospheric pressure, a small hotspot radius of $R_H=2.0$ mm with M=2 and a large $R_H=5.0$ mm with M=5 are applied. Under 10 atm, small hotspot radius of $R_H=2.0$ mm with gradient factor of M=2 are consistently applied in hotspot temperature profiles. It should be noted that the degree of hotspot thermal stratification is approximately constant as both R_H and M vary proportionally with a fixed ΔT , as seen in Fig. 1.

The initial temperature significantly impacts flame initiation results, as shown in our previous studies [12,31]. Specifically, at higher initial temperatures, low-temperature reactions become weaker and may not be able to initiate a self-sustaining cool flame ahead of the hot flame. Conversely, at lower initial temperatures, the substantial temperature rise caused by the cool flame may lead to a quicker initiation of the hot flame, resulting in a shorter duration of the double flame structure. Hence, we select an intermediate ambient temperature $T_0=700~{\rm K}$ for demonstration. As shown in Fig. 1, the configuration of the simulation is demonstrated by the initial hotspot temperature profile, which drives reaction front initiation and propagation in the subsequent stages. This work utilizes heat release rate peak locations to identify both cool and hot flame fronts, and the burnt flame speed is defined by the time rate of change in the flame position, dr/dt.

3. Results and discussion

3.1. Effects of hotspot radius and temperature under atmospheric pressure

Fig. 2 shows the temporal evolution of the flame radius indicated by peak heat release rate for lean n-heptane/air with $\phi = 0.5$. The hotspot

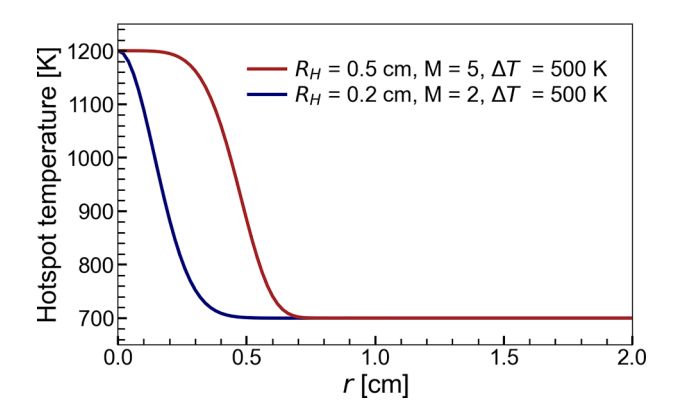


Fig. 1. Temperature distribution of hotspot with different radius but similar temperature gradient.

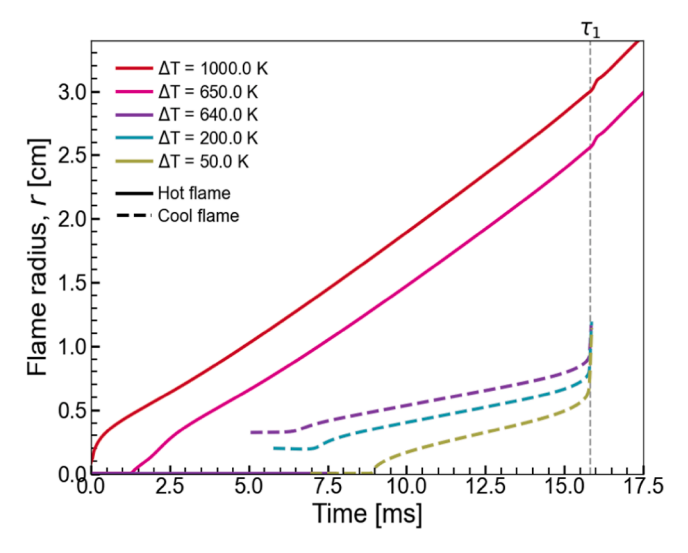


Fig. 2. Temporal evolution of flame radius with a hotspot radius of $R_{\rm H}=2$ mm and various hotspot temperature rises at initial temperature of $T_0=700$ K and atmospheric pressure for n-heptane/air mixture at equivalence ratio of $\phi=0.5$.

temperature rise, ΔT , are varied with constant hotspot radius $R_{\rm H}=2.0$ mm. It can be seen that hotspot temperatures exceeding 650 K lead to the propagation of single spherical hot flames. For $\Delta T >$ 650 K, as the hotspot central temperature T_H decreases, the induction time for hot flame initiation is delayed. For $\Delta T <$ 640 K, single spherical cool flames are initiated with a much slower propagation speed. Within the cool flame initiation regime, as ΔT decreases, the location for cool flame initiation starts to move from the edge to the center of the hotspot. Expansion of the initial radius is attributed to the sensitivity and intensity of low-temperature reactions within the hotspot.

Fig. 3 presents the time evolution of temperature and heat release rate (HRR) profiles for $\Delta T=640$ and 650 K, corresponding to the cool and hot flame initiation conditions, respectively. For both cases with $R_{\rm H}=2.0$ mm, the temperature at the center of the hotspot drops quickly due

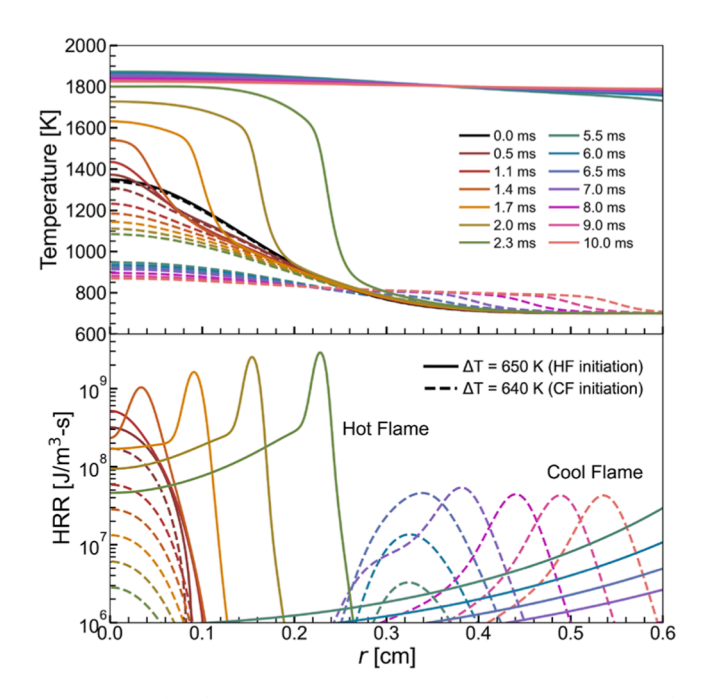


Fig. 3. Temporal evolution of temperature and heat release rate (HRR) profiles with hotspot temperature rises of $\Delta T=640$ K (Dashed line, Cool flame) and 650 K (Solid line, Hot flame) and hotspot radius of $R_{\rm H}=2$ mm at $\phi=0.5$ and $T_0=700$ K under atmospheric pressure.

to conductive and convective heat transfer into the surrounding mixture. As seen in Fig. 3, for $\Delta T=650$ K, the intense exothermic reactions occur before the hotspot temperature declines, leading to successful hot flame initiation. While for $\Delta T=640$ K, just slightly below $\Delta T=650$ K, the hotspot intensity diminishes quickly before achieving the high-temperature ignition. Consequently, the hotspot of $\Delta T=640$ K fails to trigger the hot flame propagation. However, after a certain induction period, the diminished hotspot triggers the single cool flame from r=0.3 cm, characterized by considerably lower flame temperature and HRR peak, as shown in Fig. 3.

To explore the effects of hotspot size on the cool and hot flame initiations, a larger hotspot radius of $R_{\rm H}=5$ mm is applied. Fig. 4 shows time evolution of flame radius for $R_{\rm H}=5$ mm with various hotspot temperature rises, ΔT . For $R_{\rm H}=5$ mm, the hotspot temperature required to induce hot flame propagation is reduced to 450 K, which is significantly lower than the condition with $R_{\rm H}=2$ mm. For a smaller hotspot radius, the central temperature decreases much faster, which consequently requires a higher hotspot temperature to trigger a hot flame.

At $\Delta T=450$ K slightly above the critical hotspot temperature for hot flame initiation, a cool flame is also triggered ahead of propagating hot flame. Thus, a larger hotspot with near critical hotspot temperature ensures induction time for cool flame before the hot flame, which can realize direct initiation of double flame from a hotspot. The trailing hot flame eventually catches up with the leading cool flame, and the double flame merge into a regular hot flame.

Following the results in Fig. 4, temporal evolution of temperature and heat release rate (HRR) profiles with hotspot temperature rises of $\Delta T=440~\rm K$ (Cool flame) and 450 K (Double flame) are shown in Fig. 5. Different from the single peak in HRR profile of a hot flame, HRR distribution of the double flame exhibits double-peak phenomena, which are initially separated, and gradually merged as the hot flame catches up with the leading cool flame.

Fig. 6a and 6b show burnt flame speed as a function of flame radius and flame stretch rate, respectively. As indicated by dashed lines in Fig. 6a, cool flame speed drops quickly during initial phase of ignition kernel development period. Then, the cool flame achieves a quasi-steady propagation stage. As the low-temperature ignition (LTI) approaches, the cool flame gradually evolves into the autoignition-assisted propagation mode and eventually becomes a spontaneously propagating LTI reaction front [27].

For the hot flame represented by solid lines in Fig. 6a, after the ignition kernel growth stage, the hot flame speed converges to a quasisteady limit, corresponding to the classical stretched flame regime, as

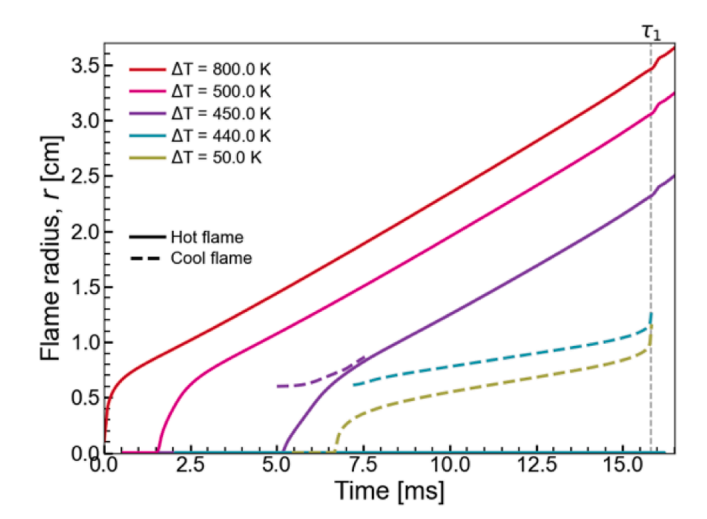


Fig. 4. Temporal evolution of flame radius with hotspot radius of $R_{\rm H}=5$ mm and various hotspot temperature rises at $\phi=0.5$ and $T_0=700$ K under atmospheric pressure.

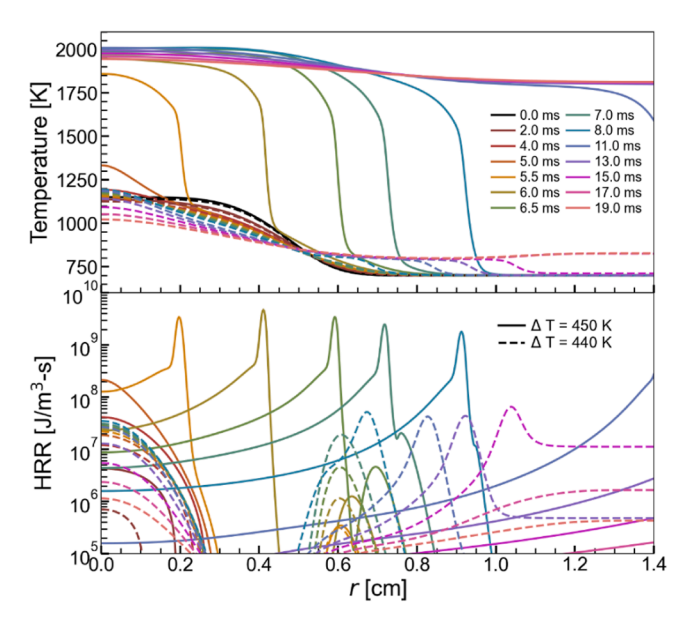


Fig. 5. Temporal evolution of temperature and heat release rate (HRR) profiles with hotspot temperature rises of $\Delta T = 440$ K (Dashed line, Cool flame) and 450 K (Solid line, Double flame) and hotspot radius of $R_{\rm H}=5$ mm at $\phi=0.5$ and $T_0 = 700$ K under atmospheric pressure.

shown in Fig. 6b. However, as LTI approaches, the hot flame speed starts to steadily increase because of non-negligible low-temperature reaction progress developed in the unburnt mixture. Upon the LTI event, there is a noticeable enhancement and fluctuation in flame speed, which is caused by the strong thermal expansion and the resulting pressure wave from the LTI. These fluctuations depend on the initiation method and configuration, and hence are not an essential part of the flame phenomenon. After the LTI, flame speed converges to second quasi-steady flame speed limit exhibiting increased flame speed and slightly weaker stretch dependence, as seen in the zoom-in plot of Fig. 6b. This is the limit corresponding to flame propagation in the post first-stage ignition mixture that is reformed by the partial equilibrium of low-temperature chemistry. The reformed mixture after the LTI has smaller molecular size of reactants, resulting in reduced effective Lewis number and Markstein length in the lean mixture. It is noted that these two quasisteady limits are independent of the hotspot characteristics, showing no memory effects on the initial condition for flame initiation. More indepth discussion on the transition of flame between these two limits and the change of flame speed and Markstein length through the LTI event has been presented in our recent study [18], and hence is not elaborated here. It is worth noting that for $\Delta T = 450$ K in Fig. 6a, during latter part of the ignition kernel expansion period prior to first quasi-steady speed limit, there is minor acceleration in hot flame speed. This observation is consistent to the previously reported over-driven flame near minimum ignition energy (MIE) condition in ignition kernel growth period [28].

From the results in this part, it should be clear that double flame initiation strongly depends on the hotspot properties. For a given mixture and ambient thermodynamic condition, a double flame can only be triggered with hotspots with sufficiently large size and intermediate value of temperature difference ΔT .

3.2. Pressure dependence of double flame initiation

In this section, we examine the effects of elevated pressure on double flame initiations from hotspot. At elevated pressures, the lowtemperature reactions become more significant primarily due to enhancement of pressure-dependent oxygen addition reactions, such as $R + O_2 = RO_2$ and QOOH + $O_2 = QOOHO_2$ [29]. Consequently, the substantial heat release from low-temperature chain reactions and the

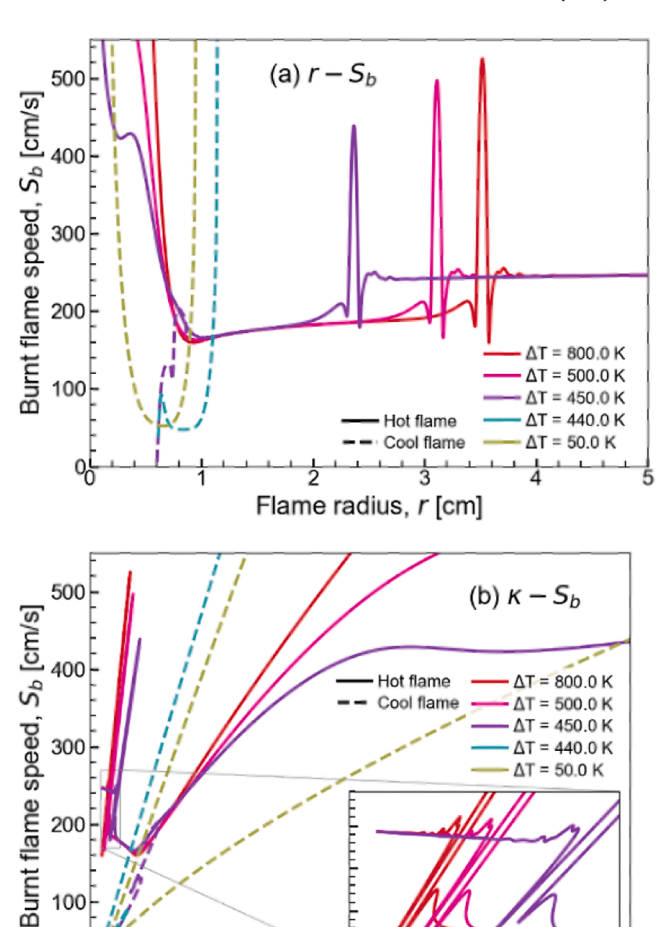


Fig. 6. Burnt flame speed as a function of (a) flame radius and (b) stretch rate with hotspot radius of $R_{\rm H}=5$ mm at $\phi=0.5$ and $T_0=700$ K under atmospheric pressure.

Stretch rate, K [1/s]

1500 2000 2500 3000 3500

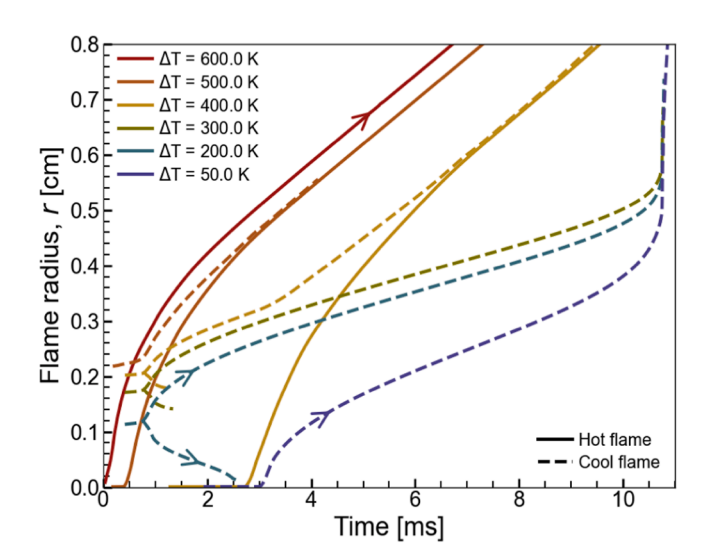


Fig. 7. Temporal evolution of flame radius with a hotspot radius of $R_{\rm H}=2$ mm and various hotspot temperature rises at $\phi = 0.5$ and $T_0 = 700$ K under 10 atm. Arrows indicate the direction of propagation - either outwardly or inwardly.

100

advanced LTI delay time at high pressure as noted by [30] enables the direct initiation of the double flame.

Fig. 7 shows the dependence of cool and hot flame evolution on hotspot temperature with $R_{\rm H}=2$ mm at $\phi=0.5$ under 10 atm. Above $\Delta T=600$ K, the single hot flame is initiated by high-temperature ignition (HTI) without any involvement of low-temperature heat release. For $\Delta T=400$ –500 K, with much longer induction time for the hot flame initiation, the heat release from the low-temperature reaction and cool flames are observed ahead of the hot flame, forming a double flame. The critical ΔT required for double flame initiation is between 300 and 400 K. For ΔT below 300 K, only cool flames are initiated, with no accompanying hot flames.

For the wide hotspot temperature range $\Delta T=200$ –500 K, cool flames are induced from the thermal boundary layer of the hotspot. As ΔT is decreased from 500 to 200 K, the initiation points of cool flame shift toward the center of the hotspot. This is because, prior to the LTI, the peak of the low-temperature heat release is constrained around 840–860 K within the hotspot. This temperature is close to the initial temperature that yields the shortest low-temperature ignition delay time at $\phi=0.5$ under 10 atm. For $\Delta T=200$ –400 K, low-temperature heat release is bifurcated at the LTI event. The bifurcated inwardly propagating cool flame travels further distance towards the center for hotspot with lower ΔT , whereas the outwardly propagating cool flame travels until either the trailing hot flame catches up with it ($\Delta T=400$ –500 K) or when the LTI occurs ($\Delta T=50$ –300 K). When ΔT is reduced to 50 K, the cool flame induction time is further delayed. Only a single cool flame is directly initiated from the hotspot center and propagates outward.

It is known that although the low-temperature ignition delay time is insensitive to the equivalence ratio, the cool flame temperature is higher for richer mixtures [30]. The variations in the thermal and chemical properties of the stoichiometric mixture especially after LTI lead to distinct double flame initiation dynamics from the lean scenario presented in Fig. 7.

Fig. 8 shows time evolution of flame radius with $R_{\rm H}=2$ mm for stoichiometric n-heptane/air mixture under 10 atm. The results indicate that both cool and hot flames can be initiated from either the thermal boundary layer at the edge of the hotspot or the center of the hotspot, with and without bifurcation, depending on ΔT . Above $\Delta T=600$ K in Fig. 8, the only hot flame starts to propagate from the center of the hotspot. At $\Delta T=500$ K, the propagation of the hot flame is followed by a cool flame initiated in the thermal boundary layer, forming a double flame structure. For $\Delta T=400$ K, with a further delay in HTI, the propagating cool flame is initiated from the edge of the hotspot, followed by the hot flame initiated from the center. For $\Delta T=300$ K, both

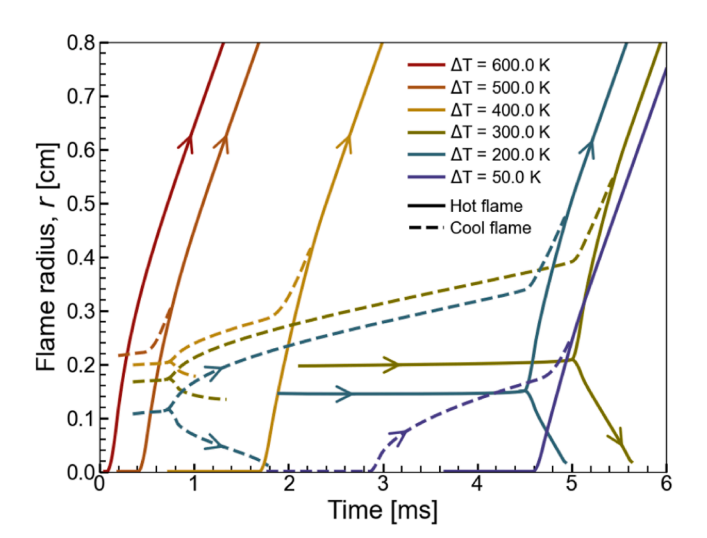


Fig. 8. Temporal evolution of flame radius with a hotspot radius of $R_{\rm H}=2$ mm and various hotspot temperature rises at $\phi=1.0$ and $T_0=700$ K under 10 atm.

cool and hot flames are initiated from the edge of the hotspot rather than the center. Interestingly, both the cool and hot flame initiation exhibit a bifurcation behavior, leading to inwardly and outwardly propagating cool and hot flame branches. At $\Delta T = 200$ K, the inwardly propagating cool flame is able to reach the center, since the hotspot temperature is below the cool flame temperature. Despite the lower hotspot temperature, the induction time for hot flame at $\Delta T = 200$ K is earlier, and the initiation location is closer to the core of the hotspot, compared to that at $\Delta T = 300$ K. This is attributed to the fact that hot flame initiations are influenced by the thermal and chemical state of the reformed mixture from cool flame propagation. At $\Delta T = 50$ K, the central temperature in hotspot is below the NTC temperature range and the LTI delay time at the center is shortest within hotspot radius. As a result, both cool and hot flames initiate from the center of the hotspot. For mixture at $\phi = 1.0$ and 10 atm, even at lower ΔT , the single cool flame cannot be induced, due to more pronounced exothermicity from the low-temperature reactions and the shorter residence time between LTI and HTI.

To further elucidate the double flame dynamics, time evolution of OH mole fraction and temperature profiles for $\Delta T=400$ and 300 K is shown in Fig. 9a and 9b, respectively. For $\Delta T=400$ K, the low-temperature reaction starts in the edge of the hotspot at t=0.6 ms and low-temperature heat release is bifurcated at the LTI event. These two bifurcated low-temperature reaction fronts propagate inwardly and outwardly respectively at t=0.9 ms. At t=1.7 ms, the inwardly propagating cool flame decays soon due to the NTC effects in the hotter region of the hotspot. Meanwhile, the outwardly propagating cool flame continues to propagate until the subsequent hot flame catches up and overtakes it after t=1.9 ms. For $\Delta T=300$ K, after the initiation (t=0.5 ms), ignition bifurcation (t=0.9 ms), and propagation (t=4.8 ms) of the cool flames, the local temperature around t=0.2 cm behind the cool flames becomes higher than that at the hotspot center. As a result, the

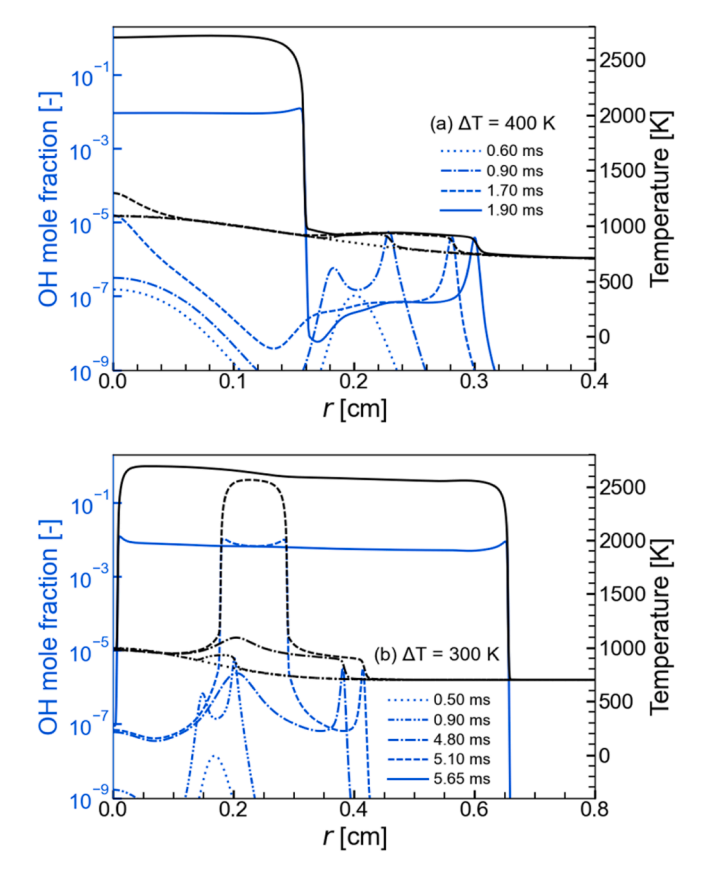
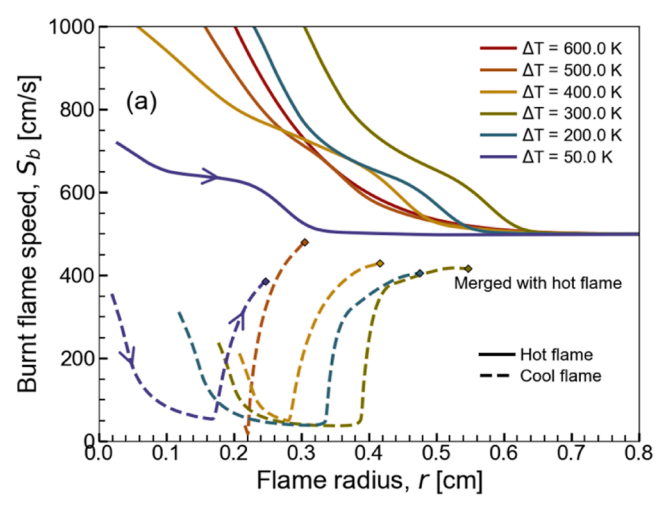


Fig. 9. Temporal evolution of OH mole fraction and temperature profiles at $\Delta T=$ (a) 400 K and (b) 300 K with $R_{\rm H}=2$ mm for a stoichiometric n-heptane/air mixture under 10 atm.

initiation of the hot flame occurs in the middle of hotspot rather than at its center, and then the hot flame is bifurcated at the HTI event and propagates in both directions. The observation of the hot flame bifurcation for the stoichiometric mixture is due to a higher LTI temperature rise relative to the lean mixture. A similar bifurcation of the hot flame following the cool flame from static hotspot has been reported in the planar transient simulation for a stoichiometric DME/O $_2$ /N $_2$ mixture with a highly increased proportion of O $_2$ at 300 K and 1 atm [12].

Now it is clear that there can be complex coupling between the leading cool flame and the hot flame initiation dynamics. In particular, the former can lead to substantial differences in initiation location and time for the latter. Fig. 10a and b show burnt flame speed of the outwardly propagating cool and hot flame branches as a function of flame radius and flame stretch rate, respectively, for stoichiometric nheptane/air mixture under 10 atm. The bifurcated inwardly propagating flames which have negative flame speed are not shown. The squared markers indicate the moments when the trailing hot flames merge with the leading cool flames. It is seen that the cool flame speed tends to approach a quasi-steady speed limit, manifested similarly as the plateau behavior shown in Fig. 6a. Such cool flame speed limit is insensitive to the hotspot intensity. As hot flame is initiated, a sudden, substantial increase in the cool flame speed is seen. Another observation is that the hot flame before merging is overdriven, whose speed is strongly boosted in the reformed mixture following the leading cool flame, and it takes a transition period after the merging instant to achieve the stretch flame



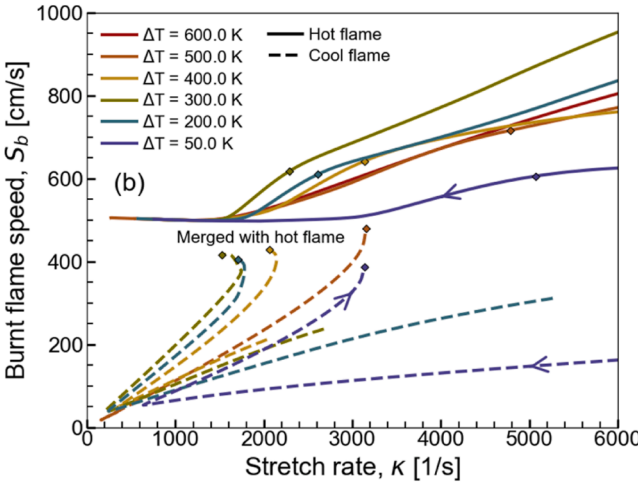


Fig. 10. Burnt flame speed as a function of (a) Flame radius and (b) stretch rate with a hotspot radius of $R_{\rm H}=2$ mm and various hotspot temperature rises at $\phi=1.0$ and $T_0=700$ K under 10 atm.

dynamics regime, where the flame speed is solely controlled by stretch.

The results in Fig. 10 further show that the interaction between cool and hot flames in a double flame structure is intermutual. At the moment of HTI, the cool flame speed undergoes a significant increase. It's a wellestablished fact that laminar flame speed relative to the static mixture, S_u , is determined from the principle of mass conservation equation: $\rho_{u}S_{u}=\rho_{b}S_{b}$ to reflect the thermal expansion effect, where ρ_{u} and ρ_{b} represent the unburnt and burnt densities, respectively. However, for the cool flame branch in a double flame structure, the cool flame speed is driven by the burnt density behind the hot flame at r = 0 cm, instead of the immediate burnt mixture following the cool flame itself. This is demonstrated in Fig. 11, where the density and temperature profiles at $\Delta T = 400$ K for a stoichiometric n-heptane/air mixture under 10 atm are shown. After the HTI, density at the center (r = 0 cm) significantly decreases, inducing substantial acceleration of the cool flame speed by the thermal expansion as shown in Fig. 10, whereas the density in the immediate burnt region of the cool flame (r ~ 0.2 -0.3 cm at 1.9 ms) is largely unchanged. The observed increase in cool flame speed has to correlate to the burnt density of the trailing hot flame. Therefore, quantitative measurement and analysis of cool flame speed involving a double flame should be based on the burnt mixture condition in the hot flame segment.

4. Conclusions

To understand initiation and propagation of double flames by a static hotspot, transient one-dimensional numerical simulations for fuel-lean and stoichiometric n-heptane/air mixture are performed in a spherical coordinate under atmospheric and elevated pressure with different hotspot characteristics.

Under atmospheric pressure, double flame is not possible for small enough hotspot sizes. As the hotspot radius increases, threshold temperature required for hot and cool flame initiation substantially decreases, and double flame initiation becomes possible for intermediate hotspot temperatures. For hotspot radius of $R_H=5\,$ mm with near critical hotspot temperature for hot flame initiation, cool flame is also triggered ahead of hot flame, resulting in the formation of the double flame structure.

With increasing pressure, dynamics of double flame initiation becomes more complicated. For lean n-heptane/air under 10 atm, single hot flame is observed for ΔT above 600 K, double flame for $\Delta T = 400-500$ K, cool flames are initiated for lower ΔT with different dynamics. Three different cool flame initiation dynamics are observed, depending on the low-temperature HRR bifurcation and the location of initiation. When temperature gradient is steep ($\Delta T = 500$ K), a cool

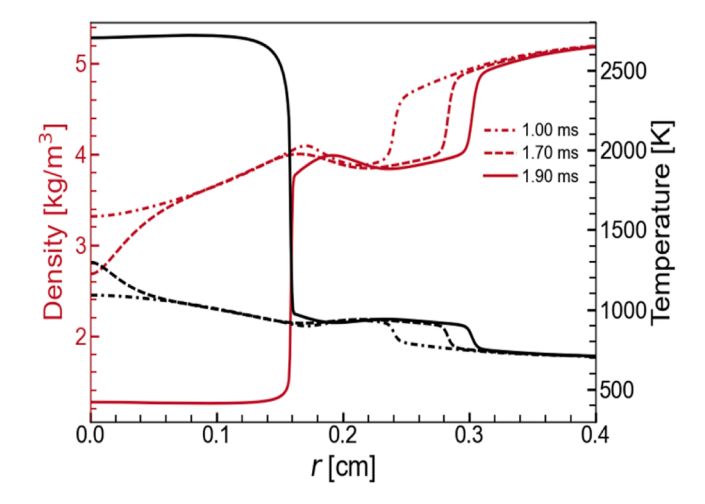


Fig. 11. Temporal evolution of density and temperature profiles at $\Delta T=400$ K with $R_{\rm H}=2$ mm for a stoichiometric n-heptane/air mixture under 10 atm.

flame first initiates from the edge of the hotspot, followed by a hot flame initiated from the center. When hotspot temperature is below NTC temperature ($\Delta T = 50$ K), a single cool flame is initiated from the center of the hotspot. Between $\Delta T = 300$ and 400 K, the bifurcation of cool flame is observed, where two cool flames are initiated from the thermal boundary layer and propagate inwardly and outwardly respectively.

For stoichiometric mixture under 10 atm, in addition to cool flame bifurcation, the hot flame can also bifurcate due to the strong LTI temperature rise. For hotspot with sufficiently low temperatures, a single cool flame is not possible, instead, a double flame will be triggered, with both cool and hot flame initiated from the center. Further thermal-chemical and flame dynamic analysis shows that the interaction of the cool and hot flames in a double flame is inherently intermutual. Hot flame in a double flame structure is overdriven, with substantially higher flame speed subject to the thermochemical change from the leading cool flame. While the cool flame speed is enhanced by the thermal expansion effect from the trailing hot flame.

Future study will cover a wider range of thermodynamic and mixture conditions for the construction of a double flame initiation regime diagram, which strongly depends on the novel double flame dynamics and interaction mechanism identified in the current study.

CRediT authorship contribution statement

Keisuke Akita: Writing – original draft, Visualization, Validation, Software, Methodology, Investigation, Formal analysis, Data curation. Peng Zhao: Writing – review & editing, Writing – original draft, Supervision, Project administration, Methodology, Investigation, Funding acquisition, Formal analysis, Conceptualization. Youhi Morii: Writing – review & editing, Supervision, Software, Methodology. Kaoru Maruta: Writing – review & editing, Supervision, Resources, Project administration.

Declaration of competing interest

The authors declare that they have no known competing financial interests or personal relationships that could have appeared to influence the work reported in this paper.

Acknowledgment

This work is supported by Grant-in-Aid for JSPS Fellows Grant Number 22J10603. We gratefully acknowledge the computational resources on AFI-NIFY at Institute of Fluid Science, Tohoku University. PZ is supported by NSF through grant number 2225803.

Novelty and significance statement

This research gives a novel understanding of how pressure and hotspot features influence the initiation and propagation of double flame dynamics. Under engine-relevant high-pressure conditions, the double flame initiation exhibits complex flame dynamics with changes in cool and hot flame bifurcation behaviors and their initiation locations. Analysis of thermochemical structure in double flame has shown that the interaction of cool and hot flames in a double flame structure is inherently mutual, in that the leading cool flame enhances trailing hot flame speed through reform of the unburnt mixture, while the trailing hot flame initiation affects the leading cool flame via thermal expansion effects. The findings in this work contribute valuable insights into fundamental double flame initiation and hotspot ignition in practical combustion applications.

References

- L. Bates, D. Bradley, G. Paczko, N. Peters, Engine hot spots: modes of auto-ignition and reaction propagation, Combust. Flame 166 (2016) 80–85.
- [2] S. Hajireza, F. Mauss, B. Sundén, Hot-spot autoignition in spark ignition engines, Proc. Combust. Inst. 28 (2000) 1169–1175.
- [3] P.D. Ronney, Laser versus conventional ignition of flames, Opt. Eng. 33 (1994) 510–521.
- [4] Z. Wang, Y. Qi, X. He, J. Wang, S. Shuai, C.K. Law, Analysis of pre-ignition to super-knock: hotspot-induced deflagration to detonation, Fuel 144 (2015) 222–227.
- [5] K. Rönn, A. Swarts, V. Kalaskar, T. Alger, R. Tripathi, J. Keskiväli, O. Kaario, A. Santasalo-Aarnio, R. Reitz, M. Larmi, Low-speed pre-ignition and super-knock in boosted spark-ignition engines: a review, Prog. Energy Combust. Sci. 95 (2023).
- [6] G. Xiao, H. Ge, P. Zhao, Initiation and propagation of one-dimensional planar flames in mixtures with variable reaction progress, Combust. Flame. 236 (2022) 111765.
- [7] X.J. Gu, D.R. Emerson, D. Bradley, Modes of reaction front propagation from hot spots. Combust. Flame 133 (2003) 63–74.
- [8] W. Zhang, M. Faqih, X. Gou, Z. Chen, Numerical study on the transient evolution of a premixed cool flame. Combust. Flame 187 (2018) 129–136.
- [9] T. Zhang, A.J. Susa, R.K. Hanson, Y. Ju, Studies of the dynamics of autoignition assisted outwardly propagating spherical cool and double flames under shock-tube conditions. Proc. Combust. Inst. 38 (2021) 2275–2283.
- [10] X. Jia, Y. Xu, H. Zheng, H. Zhang, Direct detonation initiation in hydrogen/air mixture: effects of compositional gradient and hotspot condition, J Fluid Mech 970 (2023) A22.
- [11] Y. Ju, W. Sun, M.P. Burke, X. Gou, Z. Chen, Multi-timescale modeling of ignition and flame regimes of n-heptane-air mixtures near spark assisted homogeneous charge compression ignition conditions, Proc. Combust. Inst. 33 (2011) 1245–1251
- [12] P. Zhao, W. Liang, S. Deng, C.K. Law, Initiation and propagation of laminar premixed cool flames. Fuel 166 (2016) 477–487.
- [13] A.J. Susa, A.M. Ferris, D.F. Davidson, R.K. Hanson, Experimental shock tube measurements of laminar burning velocity of n-heptane and iso-octane in the negative temperature coefficient regime, AIAA Scitech 2019 Forum (2019) 1–9.
- [14] T. Goyal, O. Samimi-Abianeh, Measurement and Simulation of Autoignition-Assisted Flame Speed of N-Heptane Mixture at Elevated Gas Temperature, Ind. Eng. Chem. Res. 62 (2023) 8719–8725.
- [15] T. Zhang, A.J. Susa, R.K. Hanson, Y. Ju, Two-dimensional simulation of cool and double flame formation induced by the laser ignition under shock-tube conditions, Proc. Combust. Inst. 39 (2023) 2017–2025.
- [16] Q. Yang, P. Zhao, Minimum ignition energy and propagation dynamics of laminar premixed cool flames, Proc. Combust. Inst. 38 (2021) 2315–2322.
- [17] L. Wang, J. Pan, H. Wei, G. Shu, Thermal and chemical effects of low-temperature chemistry on flame initiation and propagation, Combust. Flame 253 (2023) 112779
- [18] K. Akita, P. Zhao, Y. Morii, K. Maruta, D. Splitter, F. Dal, F. Chuahy, Effects of unburnt reaction progress on stretch flame dynamics under elevated temperatures, Combust. Flame 259 (2024) 113193.
- [19] J.A. Miller, R.J. Kee, F.M. Rupley, CHEMKIN-II: a Fortran Chemical Kinetics Package for the Analysis of Gas Phase Chemical Kinetics, (1989) Report No. SAND 89-8009B.
- [20] B. Van Leer, Flux-Vector Splitting for the Euler Equations, Conference on Numerical Methods in Fluid Dynamics. 170 (1982) 507–512.
- [21] E.F. Toro, M. Spruce, W. Speares, Restoration of the contact surface in the HLL-Riemann solver, Shock Waves 4 (1994) 25–34.
- [22] S. Gottlieb, C.W. Shu, Total variation diminishing runge-kutta schemes, Math Comput. 67 (1998) 73–85.
- [23] Y. Morii, E. Shima, Optimization of one-parameter family of integration formulae for solving stiff chemical-kinetic ODEs, Sci. Rep. 10 (2020) 1–13.
- [24] X. Chen, P. Zhao, P. Dai, Z. Chen, On the prediction of hot spot induced ignition by the Livengood-Wu integral, Proc. Combust. Inst. 38 (2021) 4709–4716.
- [25] K. Akita, Y. Morii, Y. Murakami, H. Nakamura, T. Tezuka, K. Maruta, Dynamics of FREI with/without cool flame interaction, Proc. Combust. Inst. 39 (2023) 1957–1965.
- [26] C.S. Yoo, T. Lu, J.H. Chen, C.K. Law, Direct numerical simulations of ignition of a lean n-heptane/air mixture with temperature inhomogeneities at constant volume: parametric study, Combust. Flame 158 (2011) 1727–1741.
- [27] A. Bhagatwala, R. Sankaran, S. Kokjohn, J.H. Chen, Numerical investigation of spontaneous flame propagation under RCCI conditions, Combust. Flame 162 (2015) 3412–3426.
- [28] Q. Yang, Z. Chen, A.J. Susa, R.K. Hanson, P. Zhao, Thermal-pyrolysis induced overdriven flame and its potential role in the negative-temperature dependence of isooctane flame speed at elevated temperatures, Combust. Flame 223 (2021) 65–76.
- [29] P. Dagaut, M. Reuillon, M. Cathonnet, Experimental study of the oxidation of n-heptane in a jet stirred reactor from low to high temperature and pressures up to 40 atm, Combust. Flame 101 (1995) 132–140.
- [30] P. Zhao, C.K. Law, The role of global and detailed kinetics in the first-stage ignition delay in NTC-affected phenomena, Combust. Flame 160 (2013) 2352–2358.
- [31] M. Tao, Q. Yang, P. Lynch, P. Zhao, Auto-ignition and reaction front dynamics in mixtures with temperature and concentration stratification, Front. Mech. Eng. 6 (2020) 68.